Chapter II Randomly Functionalized Linear Chains with Self-Associating Groups

2.1 Introduction

Suppressing misting of fluids has long been achieved in water (e.g., controlling the coherence of a water jet) and in lubricating oils (e.g., cutting fluids in large-scale machining operations) by simply introducing an extremely long linear polymer at the point of application of the fluid (e.g., in the water tanks of fire-fighting equipment or the dispensing robot in a machine shop). The unmet challenge is developing an additive that will behave like the ultralong linear chains even after the fluid has been transported, stored, and filtered. The most promising strategies emerging from the era of intensive effort on antimisting kerosene (AMK) were polymer molecules that associate with one another via functional groups statistically distributed along the chains. Unfortunately, a survey of the literature reveals that the physical phenomena whereby associations drive mist suppression are poorly understood. In the case of FM-9 polymer (Figure 1.4a), the patent literature[1] reveals an engineering approach with emphasis on practical testing, aimed at developing a working anti-misting formulation for aviation fuel by trial and error. At each step of the way additional complexity was introduced, but without commensurate generation of new understanding. The result was a formulation whose behavior and mist-control effectiveness under high rates of deformation remains a mystery.[1-3]

We begin our study of associating polymers as mist-suppressing agents with the simplest molecular design, i.e., randomly functionalized linear chains with self-associating groups similar to FM-9. To generate understanding of physical phenomena, we designed and synthesized model polymers: chains of matched length and narrow length distribution (anionically synthesized linear polybutadienes of 510 and 1250 kg/mol) were functionalized with systematically varied extent of pair-wise “stickers” (carboxylic acid side groups incorporated by grafting 3-mercaptopropionic acid to the pendant double bonds of 1,2-units in the polybutadiene chains).

The model polymers were subjected to complementary measurements to evaluate the size of the supramolecular aggregates that they form, and the consequences those aggregates have on rheological properties and mist suppression. Attention was focused on low concentration

solutions relevant to antimisting of aviation fuel. Viscosity measurements of entangled solutions are included to test existing theory of the gelation of self-association polymers. The specific viscosity results indicate a significant degree of chain collapse, which is absent from prior theoretical models; therefore, we present a theoretical treatment of chain size at infinite dilution to gain insight into the role of chain collapse.

The body of results presented here calls into question many of the widely accepted conclusions presented in the prior literature. We find that inadequate attention was given to issues of phase separation and to the compact conformations that chains adopt when they are decorated with self-associating stickers. Therefore, alternative strategies to achieve antimisting polymers that resist shear degradation are suggested.

2.2 Experimental

2.2.1 Materials

Prepolymer polybutadiene (PB) chains of weight-average molecular weight M_w = 510 kg/mol (containing ~ 98% 1,2 units and with M_w/M_n = 1.15), hereafter referred to as 510kPB, were kindly provided by Dr. Steven Smith of Procter and Gamble Company. Prepolymer PB chains of M_w = 1250 kg/mol, hereafter referred to as 1250kPB, were purchased from Polymer Source, Inc. (product ID P1914-Bd, containing ~ 8% 1,2 adducts, with M_w/M_n = 1.09). Polyisobutylene of M_w = 4200 kg/mol, hereafter referred to as 4200kPIB, was purchased from Aldrich (product number 181498, with M_w/M_n = 1.35). 2,6-Di-*tert*-butyl-4-methylphenol (BHT), 3-mercaptopropionic acid (MPA), and 2,2′-azobis(2-methylpropionitrile) (AIBN) were obtained at 99% purity from Sigma-Aldrich. AIBN was recrystallized biweekly in methanol (10 mL solvent per g AIBN) and stored at 4 ºC; all other reagents (as well as solvents) were stored at room temperature and used as received without further purification.

2.2.2 Representative Procedure for PB Functionalization with MPA

To 510kPB (3.6 g, 67 mmol of repeat units) dissolved in 175 mL tetrahydrofuran (THF) in a 500-mL Schlenk round bottom flask was added a 25 mL THF solution of MPA (0.45 g, 4.2 mmol) and AIBN (113 mg, 0.69 mmol). The contents of the Schlenk flask were degassed in 3 freeze-pump-thaw cycles, warmed to 55 ºC, and then allowed to react at 55 ºC for 105 min. Following the reaction, the polymer solution was transferred to a 500-mL jar containing

a small amount of BHT, cooled in liquid nitrogen, and precipitated by addition of 200 mL of cold methanol. The polymer was purified by reprecipitation from a THF solution (containing ca. 1 wt % BHT) with cold methanol, followed by drying to constant weight under vacuum at room temperature. Reaction conditions and results are summarized in Table 2.1 (entry 510kPB1.8A).

2.2.3 Polymer Characterization

The extent of incorporation of MPA units into PB polymer was determined by analysis of ^{1}H NMR spectra, obtained using a Varian Mercury 300 spectrometer (300 MHz). All spectra were recorded in $CDCl_3$ and referenced to tetramethylsilane. Measurements of polymer molecular weight distributions by gel permeation chromatography (GPC) were carried out in THF at 25 ºC eluting at 0.9 mL/min through four PLgel 10-μm analytical columns (Polymer Labs, 10^6 to 10^3 Å in pore size) connected to a Waters 410 differential refractometer detector (λ = 930 nm). All GPC measurements were analyzed based on calibration using polystyrene standards. Polystyrene-equivalent molecular weights determined in this manner were substantially larger for PB than values provided by the suppliers of the polymers. The latter values, which were obtained by light scattering in conjunction with GPC, are reported above.

2.2.4 Viscosity and Size Measurements

Polymer solutions for viscosity measurements were prepared by combining polymer and solvent in clean 20 mL scintillation vials which were placed on a Wrist-Action Shaker (Burrell Scientific) for up to 72 hrs to allow the polymer to dissolve fully and homogenously. For solutions of viscosities $\geq$ 10 Pa.s, homogeneity was achieved by first preparing diluted solutions using dichloromethane (DCM) as co-solvent, followed by selective and complete evaporation of the DCM under reduced pressure (this method was enabled by the > 100 ºC difference in normal boiling points between DCM and the solvents we used). Shear viscosity measurements were performed under steady-state flow using an AR1000 rheometer from TA Instruments. The following complementary geometries enabled measurements of viscosities ranging from 10^{-3} to 10^5 Pa.s: (i) an aluminum cone of 60 mm diameter, 1^o angle, and 29 μm truncation, (ii) a steel cone of 40 mm diameter, 2^o angle, and 55 μm truncation, and (iii) a steel plate of 25 mm diameter.

Polymer samples used for measurements of hydrodynamic diameter by dynamic light scattering were prepared by filtration of dilute polymer solutions through a 0.4-μm pore PTFE membrane with Acrodisc CR 25-mm syringe filters. A ZetaPALS (Brookhaven Instruments Corporation) instrument was used to perform the size measurements. Experiments were carried out using a laser source with wavelength of 532 nm, and the scattered light was collected at an angle of 90º. The built-in Particle Size Software was used to analyze the acquired raw data. Reported apparent hydrodynamic radii represent averages of 9 runs of 1 minute each.

2.2.5 Characterization of Fluid Breakup and Atomization

The elasticity and relaxation time of polymer solutions under elongational deformation was studied using capillary breakup extentional rheometry using a Thermo Haake CaBER1 instrument (measurements courtesy of Dr. Jan P. Plog of Thermo Fisher Scientific). The effect of polymer on fluid breakup was characterized using two methods. The first investigates the splashing, spreading, and breakup processes of individual drops impacting a smooth, solid surface. The second experiment involves the spraying of fuel with a simple paint gun (HUSKY Gravity Feed Spray Gun, model HDS 780) and visualizing the resulting spray pattern.

The three methods above are chosen for their complimentary advantages and limitations. For the present solutions, CaBER is restricted to $c > c_{min} > c^*$, where $c^* \approx 2500$ ppm by wt for 1250kPB in Jet-A, and droplet impact only led to breakup if $c < c_{max} < c^*$. The only method that is applicable across a wide range of concentrations spanning c^* is the spray experiment. CaBER provides the most quantitative measurements of effective extensional properties of dilute polymer solutions, but for practical purposes it is limited to the testing of solutions of sufficiently high extensional viscosity[4] (for Newtonian fluids the shear viscosity must exceed ~ 100 mPa.s; fluids of lower viscosity can only be examined if they have high elasticity, e.g., solutions of linear polymers having $M_w > 10^7$ g/mol). High-speed imaging of drop spreading and breakup generates high deformation rates ($> 10^3$ s^{-1}) and is remarkably reproducible, but analysis is difficult, and for the present polymers, concentrations below 1000 ppm were required to permit breakup. Spray experiments are strictly qualitative, in part because spray patterns on 2-dimensional surfaces vary greatly based on experimental settings such as the position of the gun relative to the surface and the air pressure. The appeal of the

method, however, is that it can be used to evaluate in a rapid, although coarse manner, the extent of mist suppression imparted by a polymer additive of *any* molecular weight at *any* concentration in solution.

Capillary breakup rheometry and its application to the measurement of elongational properties of low-viscosity elastic fluids have been established by McKinley and coworkers.[4, 5] The CaBER1 system measures the effective extensional properties of a fluid confined to a small column between parallel discs of diameter D_0 = 4–8 mm, by first imposing a rapid axial step strain of prescribed magnitude to induce a statically unstable "neck" shape, and then by measuring with a laser the thinning and breakup of the resultant filament under the action of capillary forces. Filament thinning, driven by the capillary pressure, is resisted by the extensional stress in the fluid. The principal experimental results obtained are the evolution of the midpoint diameter $D_{mid}(t)$ and the critical time to breakup. The Hencky strain ε_H and the apparent extensional viscosity η_{ext} are determined as follows:

$$\varepsilon_H(t) = 2\ln\left(\frac{D_0}{D_{mid}(t)}\right) \tag{2.1}$$

$$\eta_{ext}(t) = \frac{\sigma}{-\mathrm{d}D_{mid}/\mathrm{d}t} \tag{2.2}$$

where σ is the surface tension. As the fluid filament thins, a window of time in which D_{mid} decays exponentially is typically observed for sufficiently elastic fluids; this regime is used to extract a characteristic relaxation time λ of the fluid ($D_{mid} \sim \exp[-t/3\lambda]$).

Drop impact experiments were done in collaboration with Prof. Albert Ratner at the University of Iowa, according to methods developed in his lab.[6] Droplets of diameter 3 mm were carefully forced out of a needle (one at a time) and allowed to impact a smooth quartz surface at velocities of 3 m/s, while a high-speed, high-resolution camera captured the deformation and breakup behavior at frame rates of 4 kHz and spatial resolution of 15 μm/pixel (Figure 2.1). Criteria for characterizing breakup include investigation of the amount of splashing, the amount of fluid ejected, and the survival time of fluid filaments. The latter is most readily quantified and serves as our primary criterion for comparing differently functionalized polymers.

All spray measurements were performed according to the following conditions: Solution aliquots of volume ½ mL were sprayed in a fume hood at horizontal angle from a vertical height of 30 cm using 10 psi air pressure, and images of the sedimenting droplet pattern on the bench surface were recorded 80 cm downstream from the spraying source (Figure 2.2, top). Spray patterns for solutions of 4200kPIB polymer in Jet-A (Figure 2.2, compare with Figure 1.3) demonstrate that this simple experiment is able to expose the mist-suppressing action of known mist-suppressing materials.

2.3 Results

2.3.1 Synthesis of Acid-Functionalized Polybutadiene

Reaction of PB prepolymer according to Scheme 2.1 using reaction conditions summarized in Table 2.1 allows controlled incorporation of carboxylic acid side-groups by radical addition of MPA to the pendant double bonds of 1,2-PB units (Table 2.1, Figure 2.3). Consistent with general results for PB modification by thiol-ene coupling under similar conditions, we found that the functionalization reaction occurs with minimal degradation of the precursor material (refer to Chapter 5). Because our studies spanned several months, the stability of functionalized polymer over time was investigated. We found that cross-linking occurs slowly (Table 2.1, Figure 2.4), but that this process could be minimized by stabilizing the polymer with a small amount of BHT and storing it in the dark below 0 ºC. Under these conditions, polymer crosslinking caused M_w/M_n to increase by < 0.1 over time periods of up to 18 months. As an example, the polydispersity of 510kPB0.2A increased from $M_w/M_n \sim 1.16$ after reaction to $M_w/M_n \sim 1.24$ after 18 months, compared with $M_w/M_n \sim 1.15$ for 510kPB prepolymer.

As documented in Chapter 5, possible cyclization of neighboring 1,2-PB adducts (when present) results in the formation of 5-member ring structures, so that in fact the predominant polymer structure arising from functionalization of 1,2-PB chains at low thiol concentration is that shown in Scheme 2.1a. In other words, the 510kPB chains documented in Table 2.1 contain roughly the same number of cyclic structures as MPA groups. However, because all of the molecules which were further studied contained < 2% side-groups, it seems reasonable to expect that structural changes to the polymer backbone are of little consequence compared to the effects arising from the incorporation of the self-associating carboxylic acid functionalities. The extent of MPA incorporation was determined upon analysis of ^{1}H NMR

spectra by integration of backbone and side-group peaks, as explained in the footnotes.[7] It proved difficult to achieve target levels of functionalization by kinetic control of the reaction, due to poor reproducibility of the reaction rates (refer to last column of Table 2.1). For example, nearly identical reaction conditions were used during synthesis of 1250PB0.6A and 1250PB0.4A. Investigation of the kinetics of the radical functionalization reaction is beyond the scope of this study.

2.3.2 Phase Behavior

Incorporation of carboxylic acid functional groups onto PB chains decreases polymer solubility due to unfavorable solvent-sticker interactions. Intra- and inter-molecular polymer associations further drive phase separation of the polymer into a dense phase, which is observed to occur above a maximum MPA content (Table 2.2) even at low polymer concentrations (500-2500 ppm).

As shown in Table 2.2, the maximum MPA content that is compatible with polymer solubility increases with solvents of increasing polarity, consistent with the known decrease in the strength of associations with increasing solvent polarity.[8] Solvent effects on the maximum MPA content compatible with single-phase solutions were also consistent with solvent quality for the polymer backbone. In the least polar solvent (dodecane), the tendency to phase separate as MPA units are added is more severe for 1,4-PB than for 1,2-PB, in accord with the more favorable polymer-solvent interactions for 1,2-PB in *n*-alkanes: C_5–C_8 *n*-alkanes at 60 ºC are approximately θ-solvents for 1,4-PB (the Flory-Huggins interaction parameter is $\chi \sim 0.5$-0.6 for chains of size $\sim 10^4$ g/mol), while they are fair solvents for 1,2-PB ($\chi \sim 0.3$–0.4 for chains of comparable size).[9] In addition, the tendency for polymer phase separation was found to be lower in chlorinated or aromatic hydrocarbons (the latter are present at 10–40 % in aviation fuels such as Jet-A) than in less polar solvents, consistent with the higher affinity of the polybutadiene backbones for halogenated and aromatic solvents: at 60 ºC for both 1,2-PB and 1,4-PB chains of size $\sim 10^4$ g/mol, χ values are smaller by about 0.1 for 1-chloropentane compared to *n*-pentane, $\chi \sim 0.1$ for chloroform, and $\chi \sim 0.1$–0.2 in toluene.[9] Thus, the observed trends in phase behavior indicate that increasing solvent polarity expands the single-phase region due to the combined effects of increased solubility of the chain backbone and decreased strength of hydrogen bonding.

2.3.3 Effects of Stickers on Shear Viscosity for Homogeneous Solutions

Our first observation is that stickers cause a decrease in η_{sp} in dilute solutions and an increase in η_{sp} in semi-dilute solutions, for both 510 kg/mol 1,2-PB chains in 1-chlorododecane (CDD) (Figure 2.5, with $\phi^* \cong 0.003$ for the unfunctionalized prepolymer) and 1250 kg/mol 1,4-PB chains in Jet-A (Table 2.3, with $c^* \sim 0.25$ wt % for the unfunctionalized prepolymer). This result is evidence of the competing effects between intra- and inter-molecular interactions. On the one hand, intramolecular associations collapse chains and thereby decrease shear viscosity; this effect is dominant at dilute concentrations. On the other hand, intermolecular associations result in viscosity enhancements, and the magnitude of this effect increases with increasing polymer concentration above the overlap. The crossover of the η_{sp} vs. c curves for associating and non-associating polymer solutions depends on the competition between these two opposing effects, but occurs for all polymer investigated here at a polymer volume fraction that is greater than ϕ^* of the unfunctionalized polymer (Figure 2.5, Table 2.3).

Our attempts to isolate the effects of intramolecular associations on the conformation of individual chains by measuring the viscosity of dilute solutions were not successful. Based on the Einstein relationship,[10] the specific viscosity η_{sp} in dilute solution is proportional to the hydrodynamic volume occupied by individual chains. Therefore, in principle the collapse of individual chains can be measured by the ratio of the specific viscosity of an associative polymer solution to that of the corresponding unfunctionalized polymer solution at infinite dilution: $\lim_{c\to 0}\left[r_{\eta,sp} = (\eta - \eta_{solvent})/(\eta_{ref} - \eta_{solvent}) \right]$. In our case, however, $r_{\eta,sp}$ could be determined with good accuracy only when $\eta_{sp} > 0.5$ (which required concentrations > ½ ϕ^*) using the 60-mm cone-and-plate geometry (a Couette geometry was available, but in that case measurement accuracy suffered from poorer temperature control).

A second observation is that the magnitude of the effects of stickers on solution shear viscosity was small over the entire range from dilute to entangled concentrations. Even at polymer volume fraction above the overlap of the strands between stickers ϕ_s (such that interchain associations are more probable than intrachain associations), stickers generated enhancements in η_{sp} no larger than 10-fold for all 510 kg/mol 1,2-PB polymer solutions investigated (Figure 2.5). We were surprised to find such small increases in viscosity,

particularly at the highest degrees of functionalization and polymer concentration investigated. Indeed, for 510kPB1.8A polymer at 30 vol % in CDD, polymer concentration is twice ϕ_s, and the strand length between stickers is ~ 3000 g/mol, leading us to anticipate a dramatic viscosity increase due to the formation of an entangled thermoreversible network. The anticipated[11-13] steep increase in shear viscosity with increasing polymer concentration in the vicinity of ϕ_s, due to transitioning of intra- to inter-molecular pairing, was not observed.

Effects of solvent and temperature were evaluated in the concentration regime in which stickers increase η_0, using ϕ = 0.10. With increasing temperature the specific viscosity decreases, as expected, with stickers generally giving a stronger temperature dependence than the unfunctionalized parent polymer (Figure 2.6). Solvent effects accord with qualitative expectations: shifting from a non-polar solvent (dodecane, DD) to a slightly polar solvent (CDD) has little effect on the viscosity of solutions of the unfunctionalized polymer and strongly reduces the viscosity of the polymer with 0.4% stickers. The magnitude of solvent effects, however, was somewhat unexpected. For example, the change from DD to CDD results in larger changes in viscosity than the change from CDD to tetrachloroethane (TCE). To further place the magnitude of these effects in perspective, note that for 510kPB0.3A polymer the reduction of solution viscosity resulting from changing from DD to CDD is comparable to the reduction of viscosity produced by a 6-fold decrease of sticker content holding solvent fixed (from 510kPB1.8A to 510kPB0.3A in CDD solvent at both 8 ºC and 20 ºC). Evidently, small changes in polarity for non-polar solvents can be more important than major changes in molecular structure.

Based on existing reports of shear thickening in associative polymers,[14, 15] we examined the shear rate dependence of the viscosity. Monotonic shear thinning was observed in all but a very few cases, two of which are shown in Figure 2.7. Thickening was the exception, not the rule, and when it was found, its magnitude was not significant (rising only 20% above the zero-shear viscosity before the onset of shear-thinning). The effect was very weak compared to that described in the prior literature (see Section 2.4.1).

2.3.4 Effects of Stickers on Hydrodynamic Size

The observed viscosities indicate that coils adopt more compact configurations as stickers are added (e.g., $r_{\eta,sp}$ = 0.74 for 1250kPB0.6A polymer near the overlap concentration of the prepolymer in Jet-A; refer to Table 2.3). We wished to determine whether dynamic

light scattering measurements could be performed under sufficiently dilute solutions to accurately measure the hydrodynamic radius R_h of single, isolated chains. We found that measurement sensitivity unfortunately limited the concentration range to ≥ 0.05 wt % (~ $c^*/5$ based on unmodified 1250kPB in Jet-A). This was not sufficiently dilute to reach the single-chain limit: as shown in Table 2.4, a significant concentration dependence remains, indicating that inter-chain hydrogen-bonding contributes (making the apparent hydrodynamic size greater than that of a single chain).

2.3.5 Modeling of Chain Collapse at Infinite Dilution in θ-Solvent

Confronted by experimental limitations that precluded direct observation of the effects of intramolecular associations on individual chain dimensions, we developed a model of single-chain statistics at infinite dilution in θ-solvent. Consider a polymer chain containing N monomers and f stickers separated by $l = N/(f-1)$ monomers (meaning there are stickers at each chain end), with pairwise association of the stickers of energy εkT. Time-average properties of such a chain were calculated by tracking the evolution of the chain through a large number of bond-forming and bond-breaking events. This stochastic process corresponds to a semi-Markov chain,[16] such that a state of the process (corresponding to a state of the polymer chain) is fully specified by identifying which pairs of stickers form bonds, and the chain transitions from one state to the next by either breaking a bond or forming a new bond. Let the stickers be indexed from 1 to f (refer to Figure A.1 of Appendix A); let $\vec{R}_n - \vec{R}_m$ be the position of sticker m relative to sticker n; and let $L_{n,m}$ refer to the number of monomers in the shortest connected path between stickers n and m. Because the strand corresponding to the shortest path between stickers is unrestricted by associations and has Gaussian statistics in θ-solvent, the dimensionless root-mean-square end-to-end (1-to-f) distance for any given state is:

$$\sqrt{\left\langle R^2/b^2 \right\rangle} = L_{1,f}{}^{1/2} \tag{2.3}$$

where b is the monomer Kuhn length. The dimensionless radius of gyration of the chain in any specific state is:

$$\sqrt{\left\langle \frac{R_g^2}{b^2} \right\rangle} = \frac{1}{f \cdot b}\left(\sum_{n=1}^{f}\sum_{m=n}^{f} \left\langle \left(\vec{R}_n - \vec{R}_m \right)^2 \right\rangle \right)^{1/2} = \frac{1}{f}\left(\sum_{n=1}^{f}\sum_{m=n}^{f} L_{n,m} \right)^{1/2}. \tag{2.4}$$

Averaging over a large number of successive states and accounting for the time spent in each state yields the time-average properties, such as the average size of the chain. A full description of the model is given in Appendix A.

Computer simulations according to the above model allowed us to quantify the effects of bond strength (Figure 2.8), degree of functionalization (Figure 2.9), and chain length (Figure 2.10) on chain configuration. In addition to overall measures of coil size (chain end-to-end distance and radius of gyration), we examined the fraction of stickers that are paired (*fps*) and the average number of backbone units between paired stickers (*adps*), i.e., the distance between them along the chain in its stretched, unassociated state (Figure A.1). Model predictions show that intrachain associations reduce both the end-to-end distance and the radius of gyration (Figure 2.8-2.10), with the end-to-end distance decreasing more strongly. The reduction in coil dimensions with increasing strength of association arises from two effects: an increase in the fraction of stickers that are paired, and an increase in the fraction of "bonds" that occur between stickers that are widely separated along the backbone (Figure 2.8). Interestingly, the decrease of chain size with increasing extent of functionalization corresponds to remarkably straight lines on a log-normal plot (Figure 2.9). Finally, the increase in chain size upon increasing N at fixed l and ε does not follow a power-law (Figure 2.10), meaning that the chains do not behave as fractals.

2.3.6 Elasticity and Mist Suppression

2.3.6.1 Drop Impact Experiments

The effect of self-associating stickers on solution elasticity and drop breakup in very dilute solutions is manifested in drop impact experiments (Figure 2.11). Results for a reference solution of 4200 kg/mol PIB polymer show the famous effect of polymer elasticity in extensional deformation: at 180 ppm in Jet-A, these chains promote the formation of fluid filaments which completely suppress the ejection of satellite droplets (Figure 2.11a), in sharp contrast with the rapid fragmentation of ejected fluid in the absence of polymer (Figure 2.1b). Results for 1250kPB prepolymer at the same concentration (Figure 2.11b) reveal the pronounced effect of chain length on polymer elasticity: in contrast to the 4200 kg/mol PIB solution, there is more splashing of fluid initially upon impact, followed by rapid breakup of the ejected fluid. Nevertheless, the 1250kPB chains display sufficient elasticity to visibly hinder the necking and pinching processes involved in the breakup of individual droplets:

filaments that form between beads of fluid survive for ~ 2 ms (Figure 2.11b). The ability of 1250kPB to hinder drop breakup is reduced by incorporation of carboxylic side-groups at random positions along the chains, evidenced by a decrease in the lifetimes of fluid filaments for 1250kPB0.3A and 1250kPB0.6A solutions to 1.5 and 1 ms, respectively.

Suppression of breakup was enhanced significantly by increasing the polymer concentration (Figure 2.12): at 450 ppm, the lifetimes of fluid filaments were 2.5, 2.5, and 2 ms for solutions of 1250kPB, 1250kPB0.3A, and 1250kPB0.6A, respectively. This corresponds to a steeper increase with concentration of breakup suppression for the acid-functionalized chains than for the prepolymer. That observation begs for comparison of solution elasticity and extensional viscosity at higher concentrations. Because complete suppression of fluid breakup occurred for all 1250kPB solutions at polymer concentrations $\geq c^* = 2500$ ppm, characterization of fluid breakup at the overlap concentration and in the semi-dilute regime was conducted via spray experiments and capillary breakup experiments.

2.3.6.2 Spray and CaBER Experiments

Spray experiments for 1250kPB polymer at the overlap concentration of 2500 ppm by wt in Jet-A reveal that 0.2–0.6 mol % of carboxylic acid stickers do not shift droplet size to higher values during atomization of the fuel (Figure 2.13). This simple qualitative experiment successfully detects mist suppression by 4200 kg/mol PIB (Figure 2.2), showing a pronounced increase in drop size as concentration is increased even from 50 ppm to 200 ppm. By comparison, the drop size is remarkably insensitive to the addition of stickers to 1250kPB. In terms of mist suppression, what slight effects stickers have are unfavorable: the size of droplets appears to decrease as functionalization increases from 0 to 0.3 mol %, and only recovers to be similar to that for the unmodified polymer as functionalization is increased further to the 0.6 mol % solubility limit.

To place the above qualitative effects on a more rigorous foundation, quantitative measurements of extensional viscosity and relaxation time were attempted using capillary breakup rheology. Unfortunately, solution elasticity was too low to be measured for 1250 kg/mol 1,4-PB chains at concentrations below 1.5 wt % in Jet-A solvent (corresponding to $c = 6c^*$). CaBER results for solutions of 1250kPB0.3A and 1250kPB0.6A polymers show that, at 1.5 wt % polymer in Jet-A, associations caused 60–200% increases in the breakup

time of filaments, the solution's relaxation time, and the solution's apparent extensional viscosity (Figures 2.14 and 2.15). This amounts to considerably smaller effects of stickers on extensional viscosity than reported behavior for similar systems (Section 2.4.1, Figure 2.16c): relative to shear viscosity, the increases in relaxation time compared to the prepolymer solution were only 50% for 1250kPB0.3A and 60% for 1250kPB0.6A.

2.4 Discussion

The object of the present study is to obtain a fundamental understanding of the behavior of self-associating polymers through the study of homologous series of narrow-dispersed chains of controlled molecular properties. The effects of carboxylic-acid side-groups (pairwise "stickers") on rheological behavior were investigated as a function of number density of side-groups, polymer concentration, chain length, and solvent polarity.

2.4.1 Low-Concentration Solutions (Dilute and Unentangled Semidilute)

In contrast to the extensive literature on polymers that associate in solution through many-body interactions (such as ionic interactions in low polarity solvents or hydrophobic interactions in aqueous media), the literature on pairwise associating stickers is sparse, particularly in relation to the low concentration regime pertinent to fuel additives. Indeed, there are only two bodies of work that we have found focusing on dilute and semidilute solutions of polymer bearing pairwise, self-associating stickers: studies of ICI's FM-9 polymer[2, 3] and studies of Exxon's polyoctene copolymers[14, 15, 17] (Figure 1.4). Our experiments confirmed the reduction in shear viscosity (Figure 2.5) reported for dilute solutions ($c < c^*$ in Figure 2.16a). We found that the reduction of shear viscosity was accompanied by a reduction in the apparent extentional viscosity, as seen in drop breakup experiments (Figures 2.11 and 2.12). These behaviors are a consequence of the previously recognized phenomenon[14, 17] of chain collapse driven by intramolecular associations in dilute solutions. Computations confirm that for chains of ~ 10^4 Kuhn monomers, containing ~1 mol % side-groups that associate pairwise with energy ~ 10 kT (closely matching our 1250kPB0.6A polymer in DD), chain collapse is severe (Figure 2.10).

A number of salient rheological characteristics attributed to pairwise stickers in the prior literature are conspicuously absent in the present systems. Expected features include an extremely nonlinear increase in viscosity in the semidilute unentangled regime, pronounced

shear thickening, and strongly enhanced extensional viscosity (Figure 2.16). Plausible explanations for the discrepancies include the substantially higher MW or acid content of the molecules tested in earlier studies: the polyoctene copolymers prepared by Schulz[15, 17] had $M_n \sim 2\text{-}5 \times 10^6$ g/mol, so M_w up to $10\text{–}20 \times 10^6$ g/mol;[18] on the other hand the carboxylic acid content of FM-9 was 5–7 wt % methacrylic acid, according to the preferred composition divulged in the patent literature.[1] Different solvent-polymer and solvent-sticker interactions in the respective systems investigated are likely to contribute substantially to discrepancies among studies. Our data show that small changes in solvent polarity dramatically alter the phase behavior of non-polar polymers bearing polar stickers. Given the importance of solvent effects and the prevalence of phase separation that we observed, it is striking that the previous studies[2, 3, 14, 15, 17] do not provide solubility data. In view of the present results, we deduce that the high degree of functionalization in FM-9 would drive phase separation of the solutions; indeed, the patent literature describes the solutions as "hazy" and "opalescent."[1] As a result of the limited amount of experimental detail in the prior literature, it is impossible to determine which rheological features pertain to microscopically homogenous solutions, and which correspond to phase-separated mixtures.

Our results for solutions of concentration $\geq c^*$ uncover physical phenomena overlooked in the prior literature. We observed that at c^*, adding stickers produces measurable *reductions* in shear viscosity (Table 2.3, Figure 2.5) and in polymer-induced mist suppression in spray tests (indicative of a reduction in extensional viscosity; Figure 2.13). For $c >> c^*$ we observed that the effects of stickers on both shear and apparent extensional viscosity (Figure 2.5, Figure 2.15) were remarkably weak in comparison to those shown in Figure 2.16. These results reveal that the effects of chain collapse due to intrachain pairing are important beyond the dilute regime. This physical insight was lacking in the prior literature, according to which intermolecular interactions are believed to dominate solution behavior above c^*. The implications for mist control of aviation fuel are that self-associating polymers of acceptable solubility in the fuel are not superior to non-associating polymers even at concentrations several times above overlap.

2.4.2 Entangled Solutions

The viscosity versus concentration results we obtained for entangled solutions of 510 kg/mol PB chains (Figure 2.5) were in good agreement with the only experimental body of

work reporting on the dynamics of solutions of pairwise associating polymer:[19] Stadler and de Lucca Freitas modified anionically synthesized PB with hydrogen-bonding 1,2,4-triazolidine-3,5-dione side-groups, and reported a $\eta \sim \phi^6$ concentration dependence of zero-shear viscosity for squalene solutions of 1% modified chains of 2×10^5 g/mol, over nearly one decade in concentration corresponding to $0.1 < \phi < 1$. Note that this concentration dependence is identical to that which we observed for 510kPB1.8A polymer at volume fractions $\phi > 0.08$ in CDD (Figure 2.5). Given the $\eta \sim \phi^{5.3}$ relationship measured for unfunctionalized 510kPB prepolymer, this observed increase in the exponent of the concentration dependence of viscosity due to stickers seems very moderate.

The measured effect of self-associating, pair-wise polymer interactions on solution viscosity is much weaker than anticipated based on theoretical literature models of such systems. For example, Rubinstein and Semenov[11-13] predicted scaling exponents up to 8.5 in a concentration regime corresponding to a transition from predominantly intramolecular to predominantly intermolecular interactions (Figure 2.17, refer to footnotes[20] for a brief description of the model). For 510 kg/mol PB chains with carboxylic acid content up to 1.8 mol %, the observed shape of the viscosity vs. concentration curves was strikingly similar to that of the unmodified polymer, by comparison with model predictions (compare Figures 2.5 and 2.17).

Why the differences? First, it is difficult to meet Rubinstein and Semenov's model assumptions for homogenous solutions, particularly in term of the strength of associations for pairwise stickers. Second, the theory seems to give inadequate consideration to the effect of intramolecular interactions on the chain statistics. We discuss these two aspects in turn.

Satisfying Model Assumptions. We have already mentioned the apparent void in the literature dealing with solutions of linear polymers associating via binary interactions. In fact, for lack of a better choice, Rubinstein and Semenov[12] compared predictions of their model with experimental results of polymer systems interacting through many-body (rather than pairwise) association of hydrophobic groups in aqueous solutions. Given the binary nature of carboxylic acid associations, and equipped with the molecular control to vary bond strength, extent of functionalization, or chain length while holding other parameters constant, we felt that our materials were particularly well-suited for the testing of Rubinstein and Semenov's model predictions.

However, in spite of our best efforts in selecting the nature of the associations, the structure of the backbone, and the set of solvents, we unfortunately cannot be certain that our system is truly an experimental realization of their model. Regarding model assumptions concerning solvent quality and strengths of interactions, two key assumptions[12] underpin the concentration dependence of the viscosity of entangled reversible networks shown in Figure 2.17: the solvent is good (monomer excluded volume parameter v on the order of b^3), and associations are strong (such that $e^{\varepsilon} > l^{2.225}$). Our best estimate of the association energy for dimerization of carboxylic acids in CDD[21] corresponds to $\varepsilon \approx 8$–10. Assuming a Kuhn monomer of molar mass ~ 100 g/mol, the distances between stickers are $l \sim 180$, 55, and 30 Kuhn monomers for 0.3%, 1%, and 1.8% functionalized chains, so that the assumption of strong association is expected to hold for 510kPB1.0A and 510kPB1.8A, but is questionable for 510kPB0.3A. Further, our best estimate of the solvent quality for 510kPB chains in CDD[22] corresponds to $v/b^3 \sim 0.2$ or $\chi \sim 0.4$ (this number compares favorably with measured χ values for PB in shorter chloroalkanes reported by Alessi et al.).[9] Because Rubinstein and Semenov's theoretical treatment is limited to a description of scaling behavior without knowledge of the prefactors, it is difficult to assert from the above estimates of v/b^3 and ε that our system fully satisfies the model requirements of "good solvent" and "strong interactions."

In practice, the "good solvent" and "strong associations" assumptions defined above tend to be largely incompatible. Hydrogen-bonding systems model binary associations; however, their strengths of interaction are greatest in very non-polar solvents such as *n*-alkanes, which are marginal solvents for all common polymers. On the other hand, efforts to satisfy the assumption of good solvent by using, for instance, chlorinated hydrocarbons or aromatic solvents, compromise the strengths of hydrogen bond interactions. The relationship between the "good solvent" and "strong associations" criteria is further complicated by solvent-sticker interactions: Quantitative pairing of the stickers in a system requires low values of l and high values of ε, meaning high levels of functionalization with stickers exhibiting very favorable sticker-sticker interactions and, unfortunately, unfavorable sticker-solvent interactions. In this case, phase separation of the functional chains driven by adverse solvent-side group interactions is likely to occur regardless of solvent quality for the polymer backbone itself. These solvent-side group interactions which significantly impact the solubility and phase

behavior of functionalized chains were not accounted for in Rubinstein and Semenov's model.

Role of Intrachain Associations. The effect of chain collapse even above c^*, unnoticed in previous experimental work (Section 2.4.1), was also overlooked in theoretical descriptions of self-associating polymer systems. Specifically, Rubinstein and Semenov's theory fails to account for the effects of intramolecular bonds on the chains statistics. Intrachain associations are physical cross-links that cause polymer molecules to collapse onto themselves, even at concentrations >> c^*, so that expressions for segment sizes and relaxation times that are applicable to linear chains without stickers no longer hold for self-associating polymer molecules. As a result, corrections must be made to expressions of chain size R, correlation length ξ, number of monomers per correlation blob g, Zimm time of correlation blobs, tube length $a(\phi)$, etc.; Rubinstein and Semenov did not make such corrections. Calculations of chains collapse (Figures 2.8–2.10) confirm the intuitive expectation that the changes in polymer configuration due to same-chain associations are substantial, especially for long chains and strong associations.

2.5 Conclusion

The results of this study challenge the pre-existing understanding of the rheology of self-associating polymers (Figures 2.16 and 2.17), and suggest that previously accepted assertions regarding the effects of pairwise stickers on the rheology of polymer solutions deserve re-evaluation. Properly controlled studies (using functionalized and unmodified polymer homologues of matched, well-defined length) that include light scattering and rheological characterization can provide definitive tests of prior beliefs.

For 510 kg/mol and 1250 kg/mol PB chains of low polydispersity, we find that incorporation of carboxylic acid side-groups results in a strong tendency for phase separation, and observe that for homogeneous solutions, enhancements in shear and extentional viscosity due to stickers are relatively small even at polymer concentrations >> c^*, in contrast with prior expectations. Our results reveal that the effects of chain collapse due to intrachain pairing are important beyond the dilute regime—behavior unaccounted for in earlier experimental and theoretical studies. The implications for mist control of aviation fuel are that self-associating polymers of acceptable solubility in the fuel are not superior to non-associating polymers even at concentrations several times above overlap. Therefore,

alternative strategies to improve antimisting based on polymer associations in dilute solutions are needed. In the next chapter, we consider randomly functionalized linear chains bearing complementary stickers (Figure 1.7.2).

2.6 Figures, Schemes, and Tables

(a)

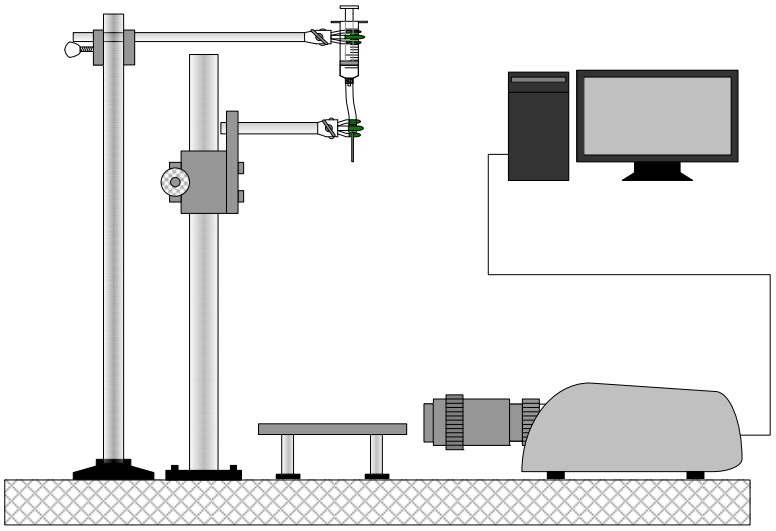

(b) Jet A solvent, 0.25 ms intervals, 15 μm/pixel resolution

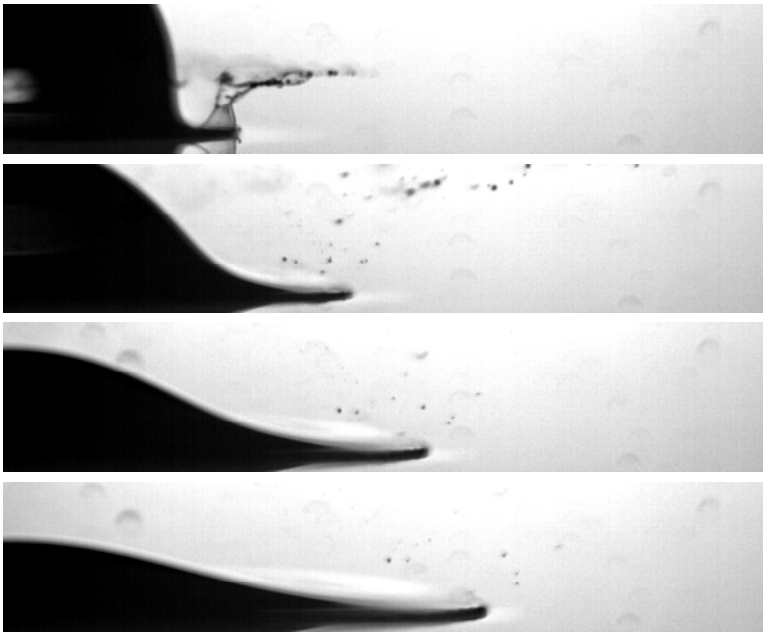

Figure 2.1 Experimental apparatus for the characterization of drop splashing, spreading, and breakup (a), and results for Jet-A solvent (b). Notice that the ejected fluid breaks up so quickly that only a small number of individual droplets can be resolved after 0.5 ms.

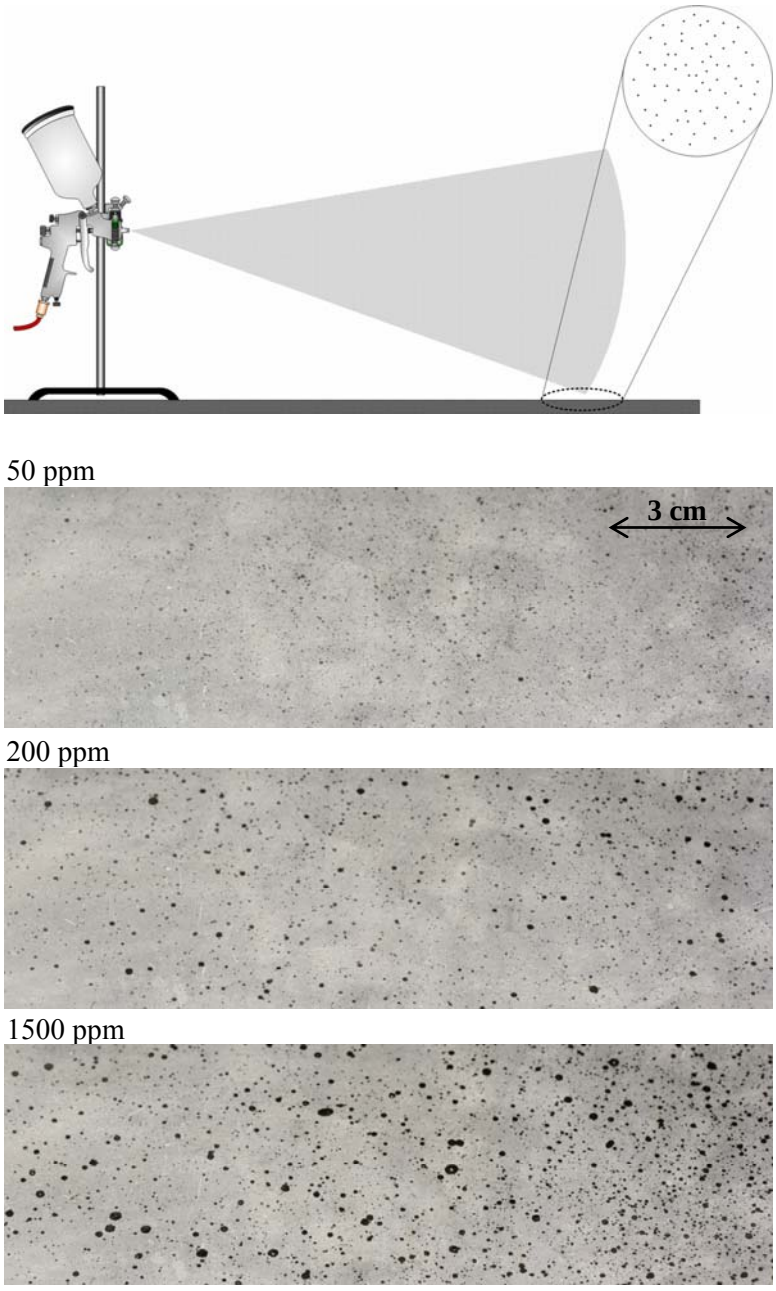

Figure 2.2 Experimental apparatus for the characterization of fuel atomization during spraying (top), and spray patterns for reference solutions of 4200 kg/mol polyisobutylene polymer at increasing weight fraction in Jet-A (bottom three photographs). Pure Jet-A is atomized so finely that there is no observable spray pattern: the fine mist is entrained by the upward air flow of the fume hood and does not settle onto the surface.

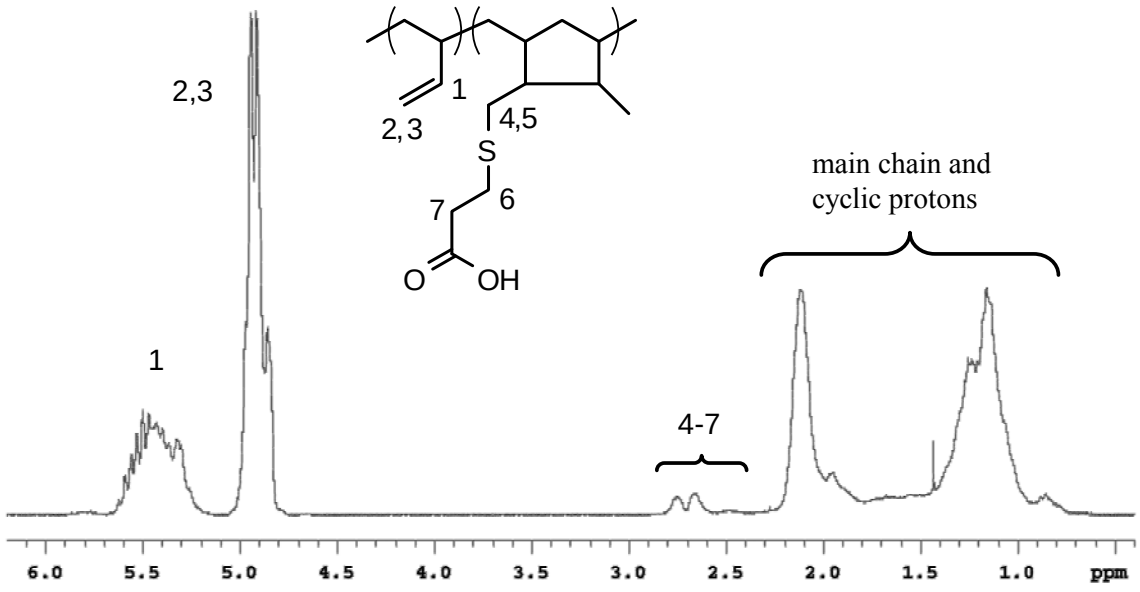

Figure 2.3 Representative ^{1}H NMR spectrum of acid-functionalized polybutadiene polymer (510kPB1.8A, refer to Table 2.1). Note that protons 4 and 5 are not equivalent.

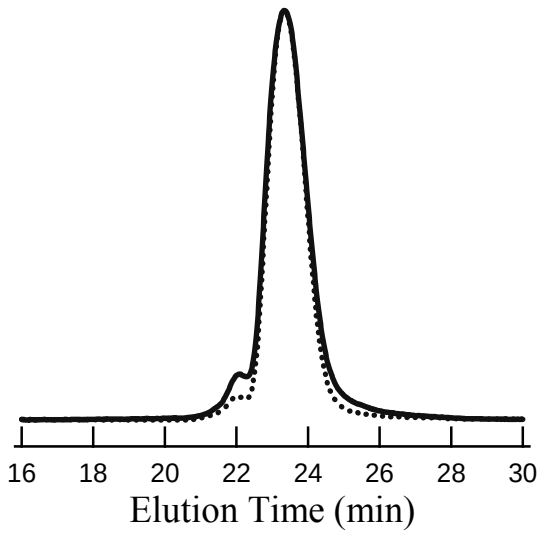

Figure 2.4 Representative gel permeation chromatography trace of acid-functionalized polybutadiene polymer. The solid line corresponds to 1250kPB0.2A (after 10 months of storage; refer to Table 2.1); the dashed line is 1250kPB prepolymer.

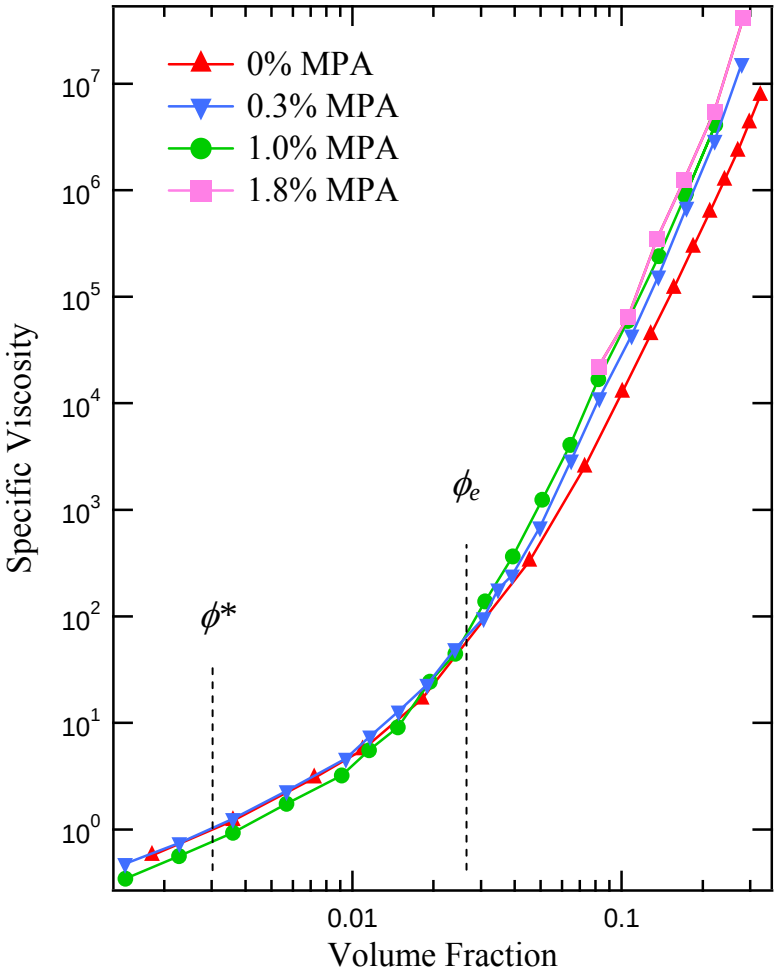

Figure 2.5 Zero-shear specific viscosity ($\eta_{sp} \equiv \eta_{solution}/\eta_{solvent} - 1$, where $\eta_{solvent}$ = 2.72 mPa.s) of 510 kg/mol 1,2-polybutadiene chains in chlorododecane at 20 ºC, as a function of 3-mercaptopropionic acid (MPA) content. For 510kPB prepolymer, the overlap concentration corresponds to $\phi^* \cong 0.003$ according to the criterion $[\eta]\phi^* \cong 1$, and the entanglement concentration is $\phi_e \cong 0.026$ (determined as the intersection of the semi-dilute and entangled regimes, corresponding to $\eta_{sp} \sim \phi^{1.3}$ and $\eta_{sp} \sim \phi^{5.3}$ regimes, respectively). The overlap concentrations of the strands between stickers were determined using the expression[23] $\phi_s = \phi^*(MW_{chain}/MW_{strand})^{-0.76}$ to be ϕ_s = 0.04, 0.10, and 0.15 for polymer chains containing 0.3%, 1.0%, and 1.8% MPA side-groups, respectively.

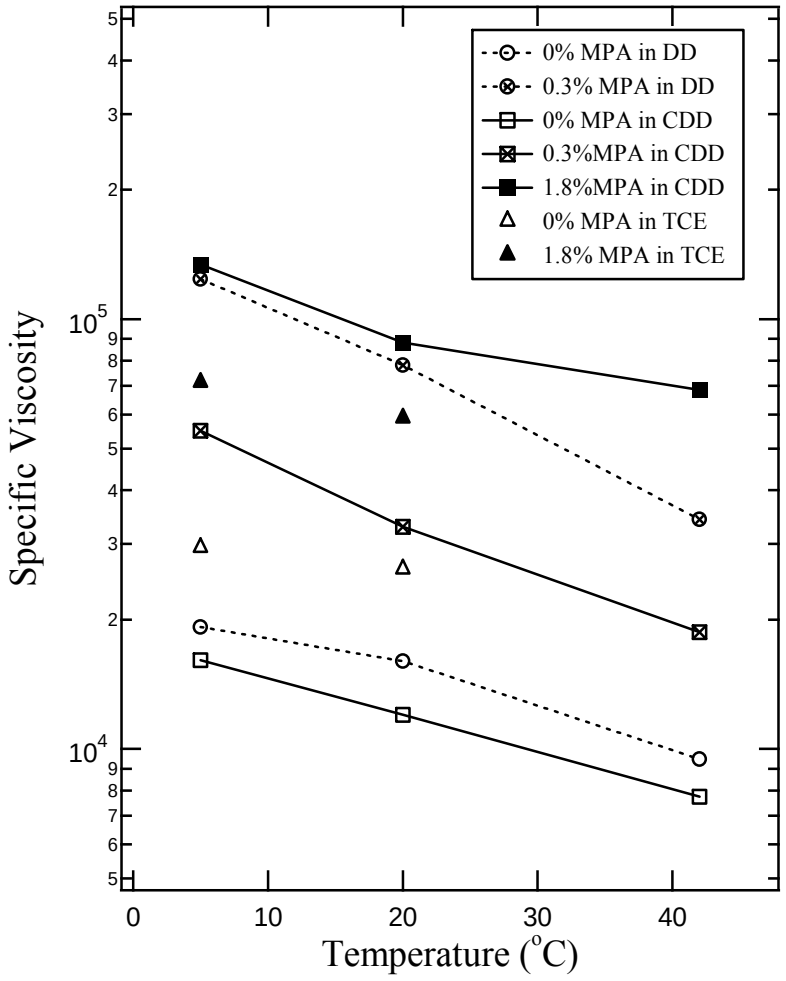

Figure 2.6 Temperature and solvent effects on specific viscosity ($\eta_{sp} \equiv \eta_{solution}/\eta_{solvent} - 1$) of 10 vol % solutions of 510 kg/mol 1,2-polybutadiene chains as a function of mercaptopropionic acid (MPA) content. Note that experiments in TCE were limited to temperatures ≤ 20 ºC due to solvent volatility, and that experiments with 1.8% stickers were not possible in DD due to phase separation.

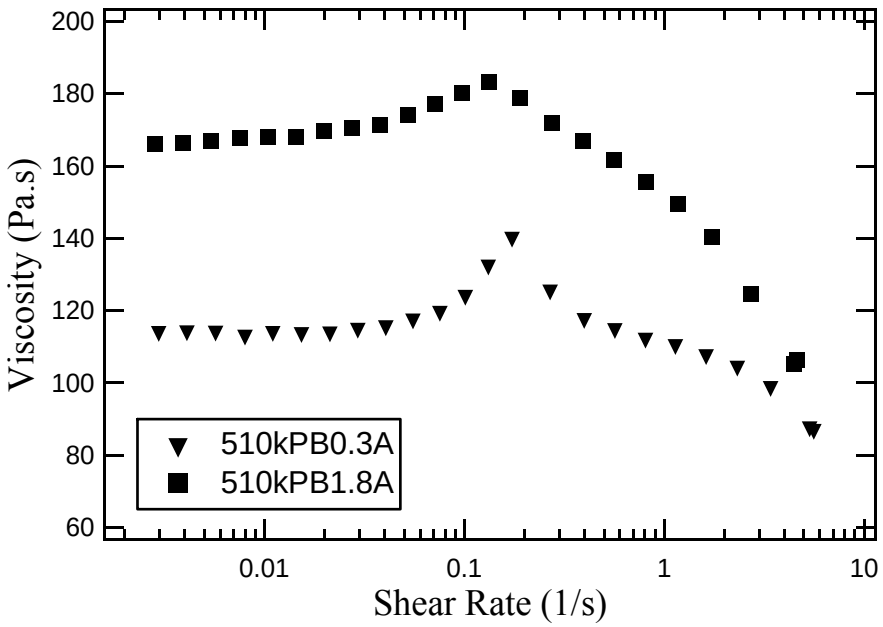

Figure 2.7 Shear viscosity as a function of shear rate for 10 vol % 510 kg/mol 1,2-polybutadiene solutions in tetrachloroethane at 20 ºC.

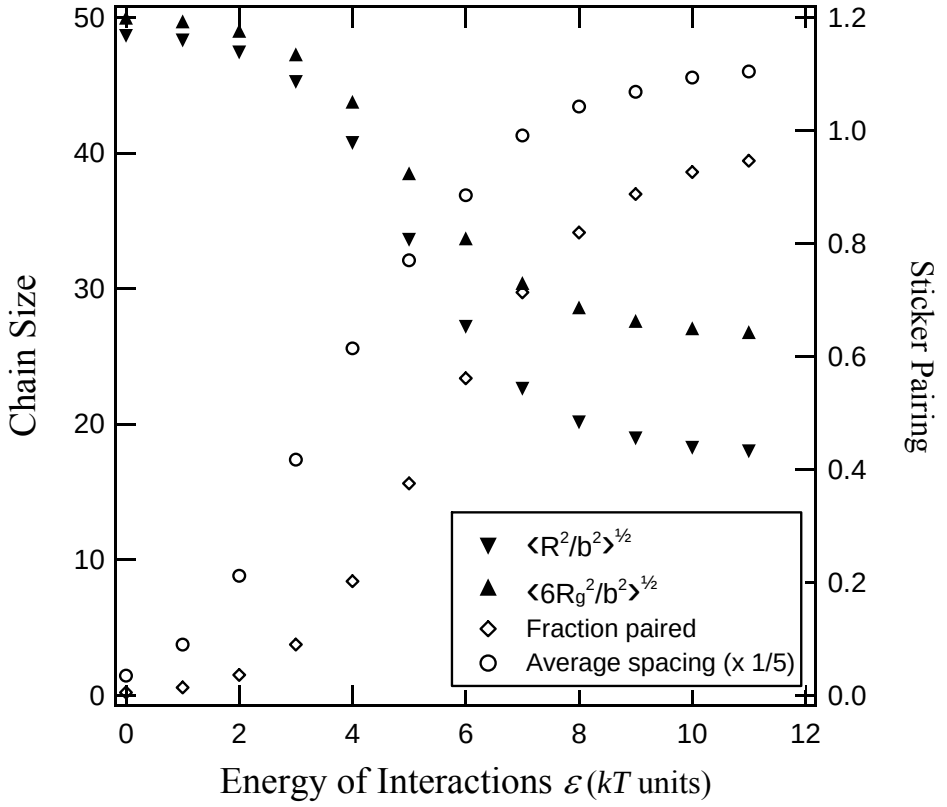

Figure 2.8 Simulation results of the end-to-end distance, radius of gyration, fraction of stickers paired (*fps*), and average spacing between paired stickers (*adps* = $\langle p\text{-}p' \rangle$, where p and p' are the indexes of stickers involved in pairs; refer to Figure A.1 of Appendix A), as a function of energy of interaction εkT for a chain with $f = 25$ stickers and $l = 100$ monomers between stickers. The bond volume was taken to be $V_b = b^3$, and the time-evolution of the chain was tracked over 2×10^5 bond-breaking or bond-forming events.

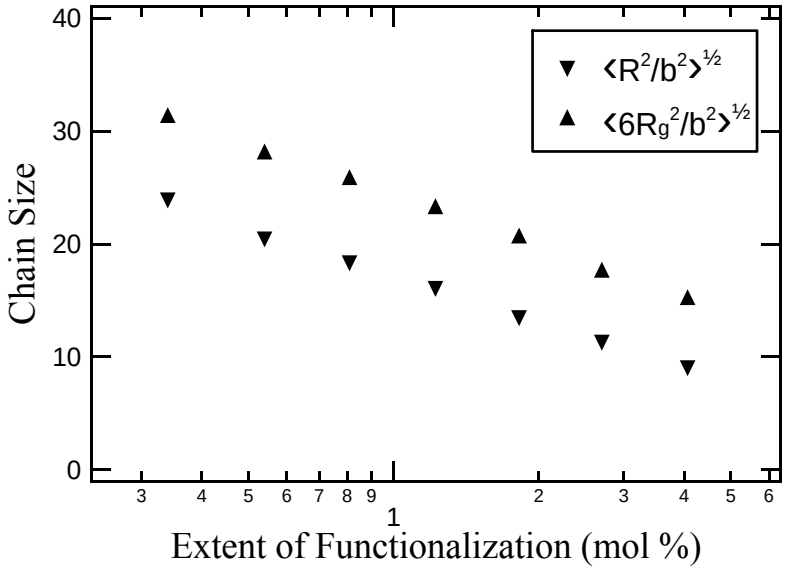

Figure 2.9 Simulation results of the end-to-end distance and radius of gyration as a function of the fraction of monomers bearing stickers (in mol %) for a chain with $N = 1500$ monomers at fixed energy of interaction $10kT$. The bond volume was taken to be $V_b = b^3$, and the time-evolution of the chain was tracked over 4×10^4 bond-breaking or bond-forming events.

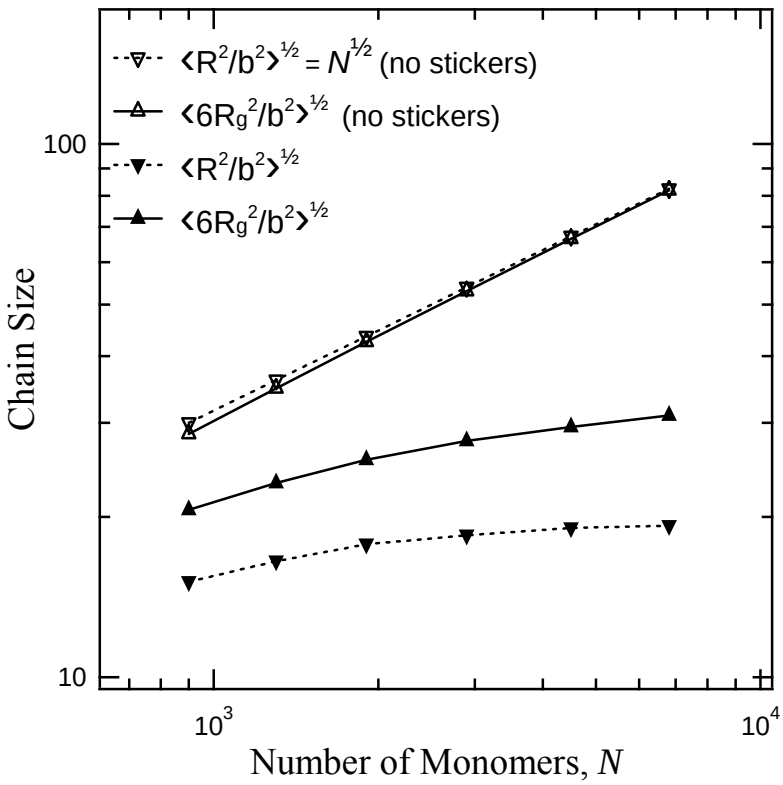

Figure 2.10 Simulation results of the end-to-end distance and radius of gyration as a function of chain length for a chain at fixed l = 100 and fixed energy of interaction 10kT (under these conditions the stickers spend the majority of their time in pairs). Open symbols correspond to chain size, calculated using Equations 2.3 and 2.4, for chains of matched length without stickers. The bond volume was taken to be $V_b = b^3$, and the time-evolution of the chain was tracked over 10^5 bond-breaking or bond-forming events.

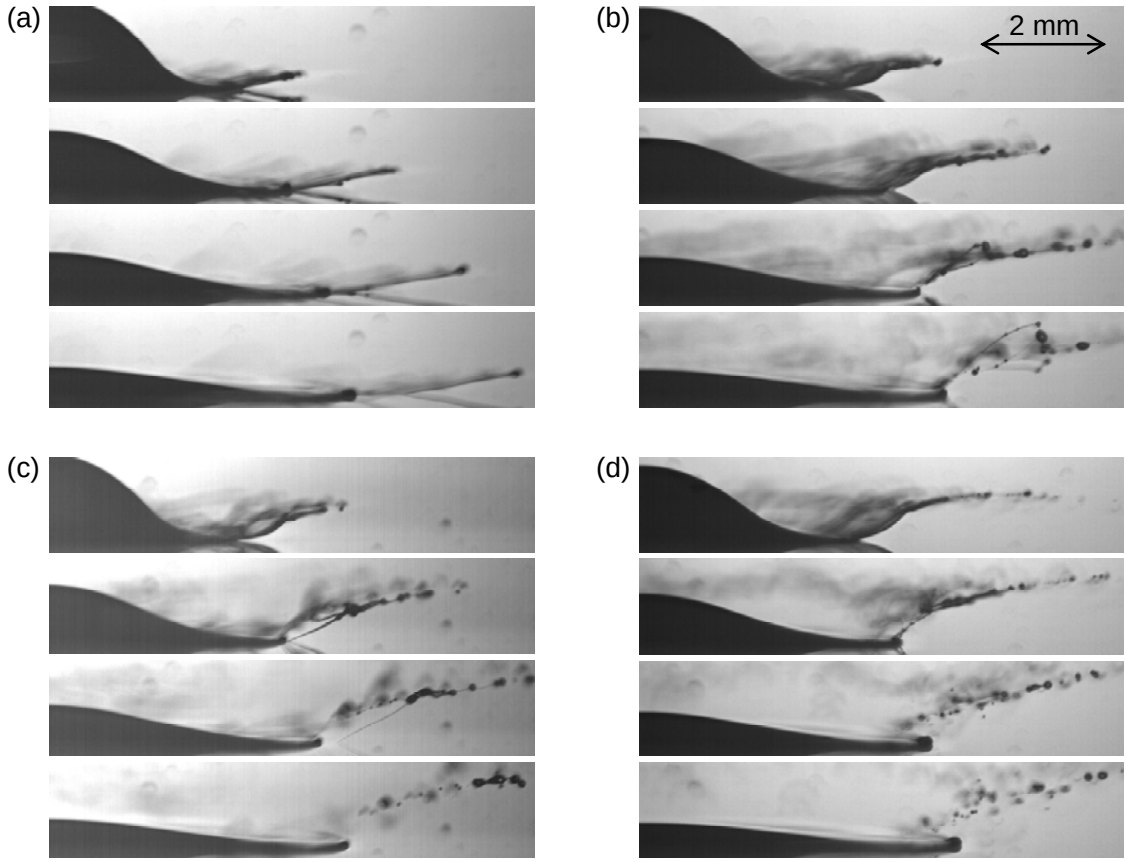

Figure 2.11 High-speed imaging of drop breakup of polymer solutions at 180 ppm by wt in Jet-A: (a) 4200 kg/mol linear, non-associating polyisobutylene chains; (b) 1250 kg/mol linear, unfunctionalized 1,4-polybutadiene chains; (c) 1250kPB0.3A chains; and (d) 1250kPB0.6A chains (refer to Table 2.1). For 4200kPIB, satellite droplets were never fully ejected; on the other hand all visible fluid filaments connecting "beads" of fluid together had broken 2 ms, 1.5 ms, and 1 ms after impact for solutions b, c, and d, respectively. The interval between frames is 0.25 ms in all cases.

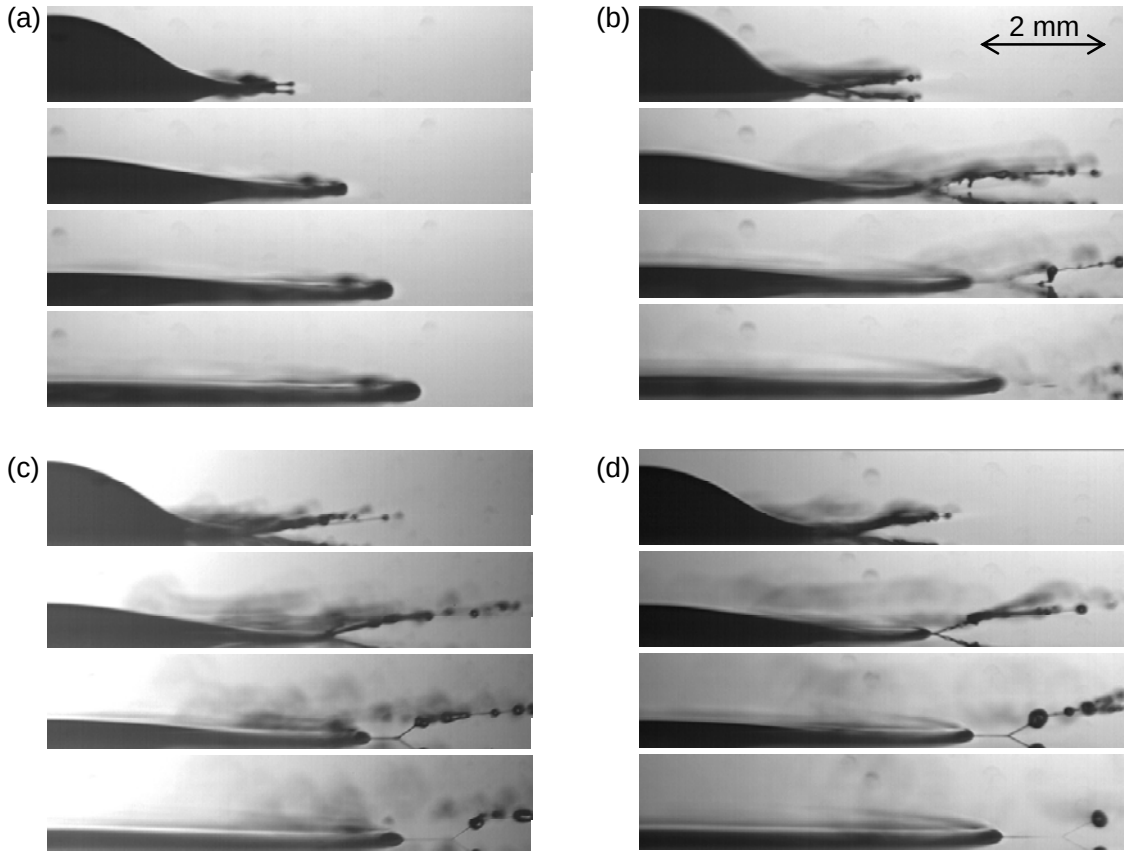

Figure 2.12 High-speed imaging of drop breakup of polymer solutions at 450 ppm by wt in Jet-A: (a) 4200 kg/mol linear, non-associating polyisobutylene chains; (b) 1250 kg/mol linear, unfunctionalized 1,4-polybutadiene chains; (c) 1250kPB0.3A chains; and (d) 1250kPB0.6A chains (refer to Table 2.1). For 4200kPIB, there is nearly complete suppression of breakup, without formation of satellite droplets; on the other hand all visible fluid filaments connecting "beads" of fluid together had broken 2.5 ms, 1.25 ms, and 0.75 ms after impact for solutions b, c, and d, respectively. The interval between frames is 0.5 ms in all cases.

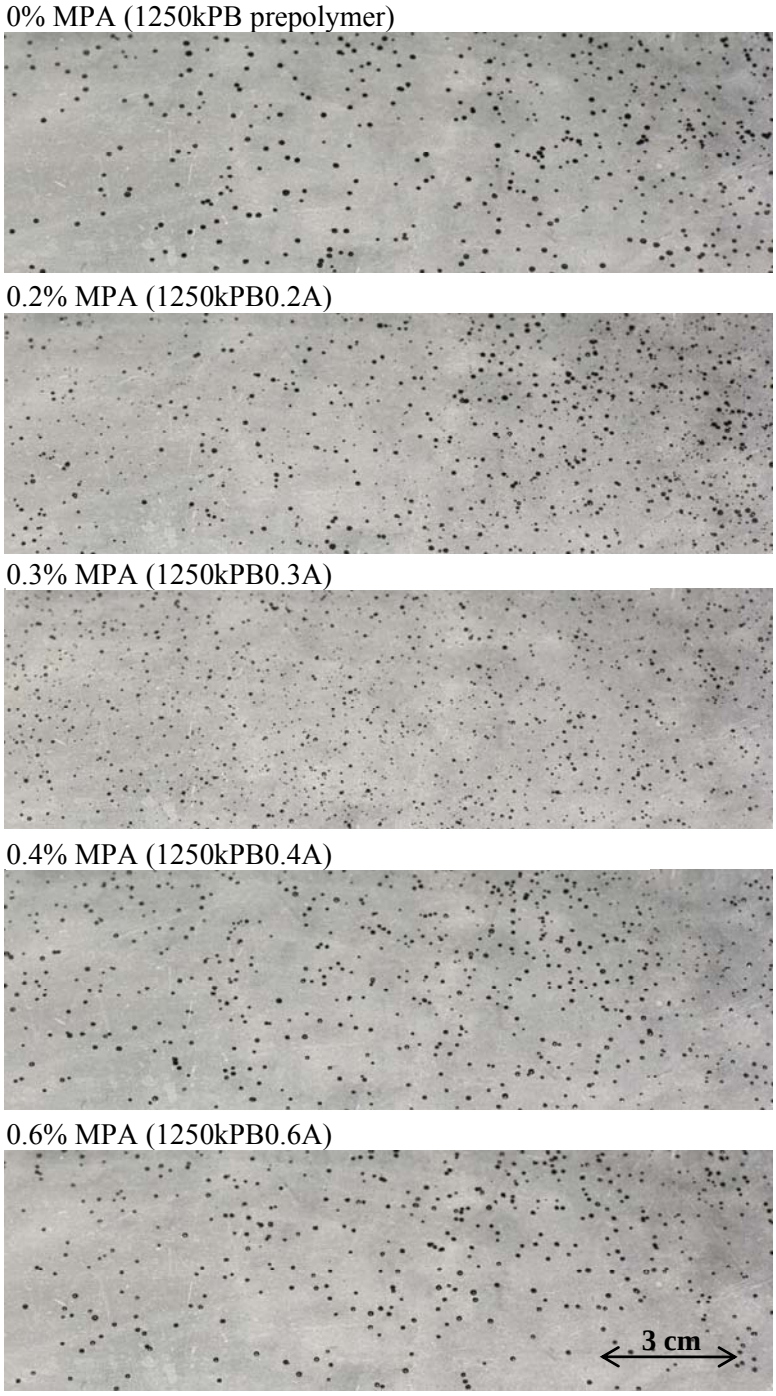

Figure 2.13 Spray patterns of solutions of 1250 kg/mol 1,4-polybutadiene chains (refer to Table 2.1) at 2500 ppm by wt in Jet-A as a function of increasing mercaptopropionic acid content.

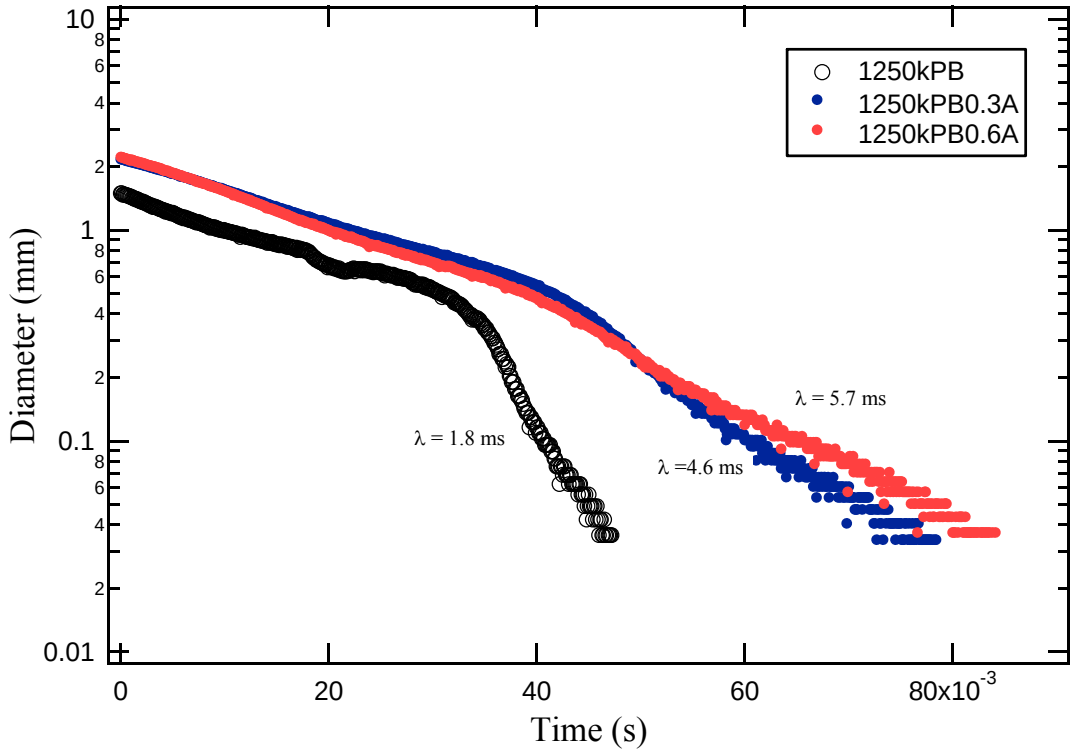

Figure 2.14 Time evolution of filament diameter during capillary breakup experiments for 1250kPB, 1250kPB0.3A, and 1250kPB0.6A polymers at 1.5 wt % total polymer content in Jet-A (corresponding to $c = 6c^*$ for 1250kPB prepolymer). All tests were performed with 8 mm diameter plates, at initial and final aspect ratios of 1.0 and 2.5, respectively. Solution shear viscosities were 48 mPa.s, 83 mPa.s, and 95 mPa.s for the 1250kPB, 1250kPB0.3A, and 1250kPB0.6A solutions, respectively. The characteristic relaxation times of the solutions, determined from the slope of the exponential decay of the filament diameter vs. time, are represented on the figure.

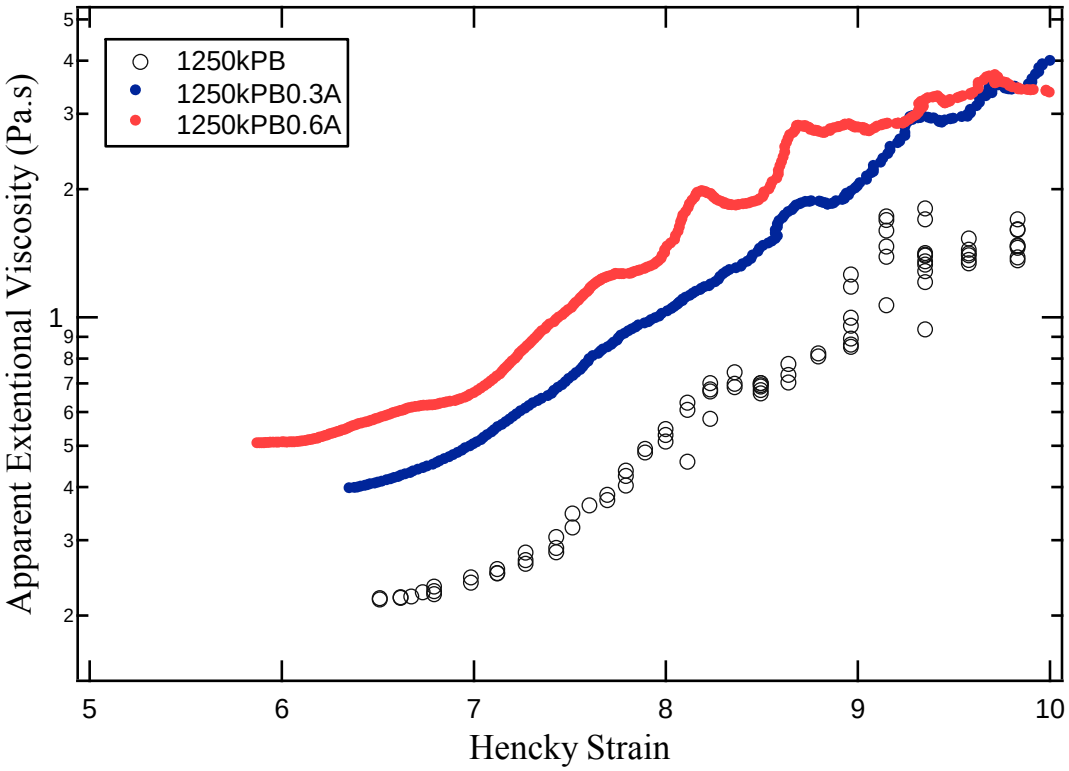

Figure 2.15 Effect of pairwise, self-associations on apparent extentional viscosity during capillary breakup rheology (refer to Figure 2.14 for experimental details).

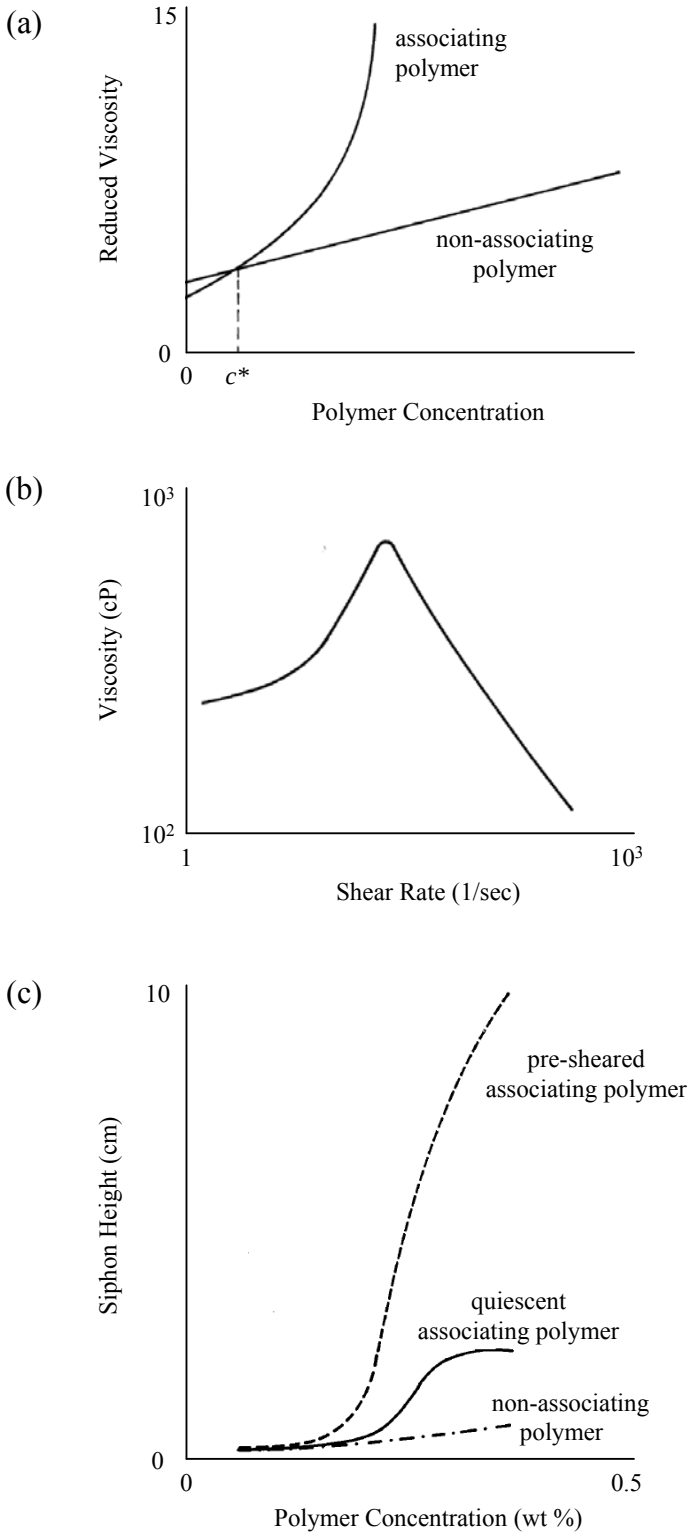

Figure 2.16 Prior understanding of the physical properties of solutions of self-associating polymer of low concentrations, according to Schulz et al.[14] Siphon height is a measure of extensional viscosity.[24] (Reproduced with permission.)

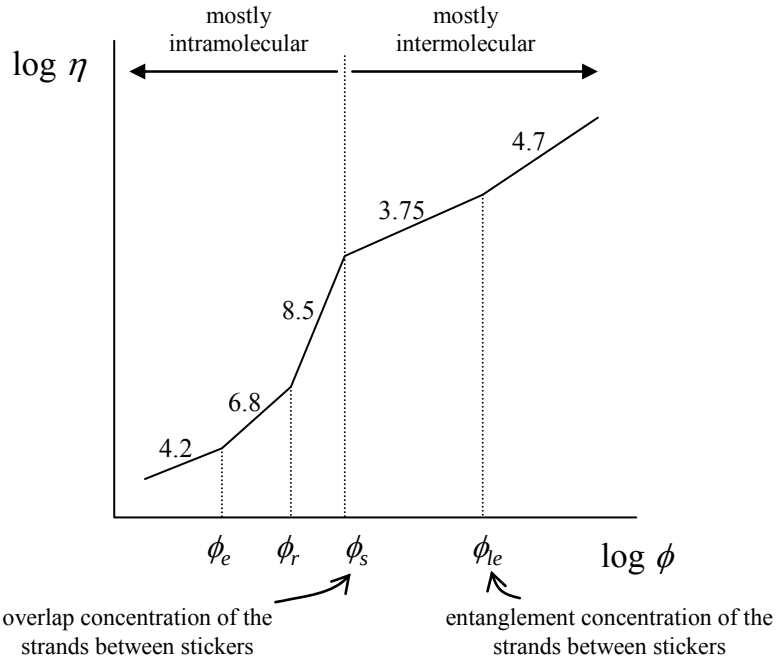

Figure 2.17 Predictions of Rubinstein and Semenov's model[12] for the concentration dependence of the viscosity of entangled reversible networks in good solvent. (Reproduced with permission. Refer to footnotes[20] for identification of the crossover concentrations). The numbers above each line segment indicate the predicted scaling exponent.

Scheme 2.1 Synthesis of Acid-Functionalized Derivatives of Polybutadiene Polymers Containing 98% 1,2 Adducts (a) and 8% 1,2 Adducts (b)

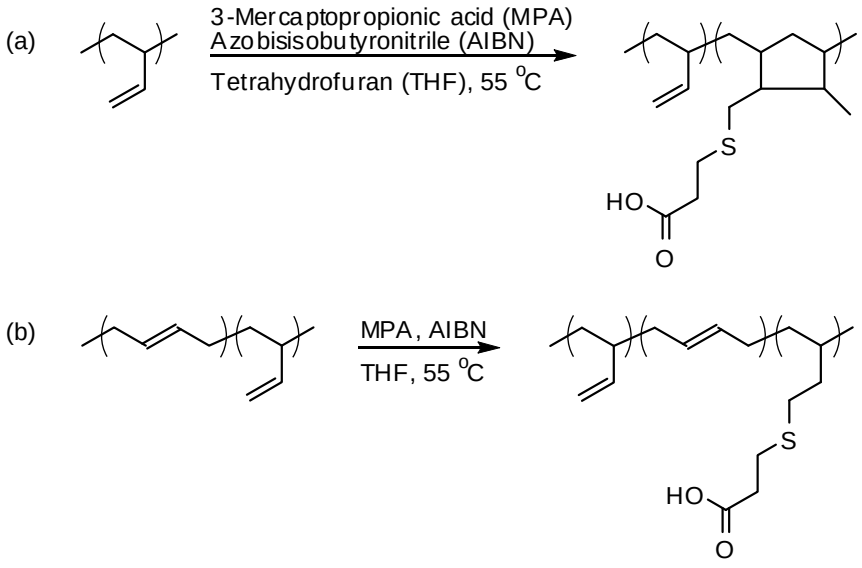

Table 2.1 Reaction Conditions and Results for Polybutadiene Functionalization with 3-Mercaptopropionic Acid

Entry[a]	[PB] (g/mL)	[MPA][b]	[AIBN] (mg/mL)	Rxn time (hrs)	Funct.[c] %	PDI[d]	rxn rate[e] ($mL^{3/2}/mol^{3/2}$ s)
510kPB0.2A	0.016	0.023	0.52	1.2	0.2	1.24	37
510kPB0.3A	0.016	0.021	0.52	2.5	0.3	1.20	30
510kPB1.0A	0.020	0.040	0.65	1.7	1.0	1.23	55
510kPB1.8A[f]	0.018	0.064	0.57	1.8	1.8	1.28	73
510kPB4.7A	0.017	0.13	0.52	1.5	4.7	1.23	130
510kPB7.1A	0.014	0.16	0.49	1.6	7.1	1.28	170
1250kPB0.2A[g]	0.010	12	0.46	0.58	0.2	1.15	41
1250kPB0.3A	0.009	16	0.62	0.55	0.3	1.29	44
1250kPB0.4A	0.009	16	0.52	1.1	0.4	1.17	35
1250kPB0.6A	0.009	16	0.54	1.2	0.6	1.23	43

[a]Functionalized PB polymers were named so that the prefix corresponds to the molecular weight of the precursor chain, and the suffix represents the mol percent of monomers bearing pendent acid groups. [b]In molar equivalent of 1,2-PB units, which are 98% of the units of 510kPB and 8% of the units of 1250kPB. [c]Molar fraction of functionalized monomers based on the total number of PB monomers (both 1,2 and 1,4 units). [d]Reported values correspond to aged samples (12-18 months for 510kPBxxA polymers, and 6-12 months for 1250kPBxxA polymers), and reflect the slow cross-linking of the polymer chains that occurs with time upon storage (see text). The 510kPB and 1250kPB prepolymers had PDI values of 1.15 and 1.09, respectively. [e]Average reaction rate divided by [1,2PB units][MPA][AIBN]$^{1/2}$. [f] ^{1}H NMR spectrum is shown in Figure 2.3. [g]GPC trace is given in Figure 2.4.

Table 2.2 Solubility Constraint on Functionalization with 3-Mercaptopropionic Acid (mol % Monomer Basis) in Various Solvents at Room Temperature

	510k 1,2 PB[a]	1250k 1,4 PB[b]
Dodecane	1.0% < < 1.8%	< 0.2%
Chlorododecane	1.0% < < 1.8%	> 0.6%
Jet-A	1.0% < < 1.8%	> 0.6%
Tetrachloroethane	1.8% < < 4.7%	> 0.6%
Chloroform	4.7% < < 7.1%	> 0.6%

[a]The lower degree of functionalization was found to be soluble at all concentrations tested; the upper degree of functionalization exhibited phase separation at low concentrations (500-2500 ppm). [b]Four degrees of functionalization were examined for 1250kPB (Table 2.1): none were soluble at low concentration (500-2500 ppm) in dodecane; all were soluble in the other solvents.

Table 2.3 Zero-Shear Specific Viscosity[a] of 1250 kg/mol 1,4-Polybutadiene Chains as a Function of 3-Mercaptopropionic Acid Content and Concentration in Jet-A at 25 ºC

c (wt %)	0% A	0.2%A	0.3%A	0.6%A
0.25	1.04	0.99	0.92	0.77
0.5	2.7	3.0	2.8	2.4
1.5	32	42	56	65

[a] $\eta_{sp} \equiv \eta_{solution}/\eta_{solvent} - 1$, where solvent viscosity was 1.45 mPa.s. Measurement reproducibility was typically within 0.03 mPa.s or 3% of the measurement (whichever is greater).

Table 2.4 Normalized Apparent Hydrodynamic Radii of Functionalized 1250 kg/mol 1,4-Polybutadiene Chains in Jet-A and Chlorododecane (CDD)[a]

	0.2%A[b]		0.3%A[b]		0.4%A[b]		0.6%A[b]	
c (by wt, in ppm)	Jet-A	CDD	Jet-A	CDD	Jet-A	CDD	Jet-A	CDD
500	1.02	-	1.07	0.95	1.07	1.02	1.06	0.91
900	1.03	-	1.10	0.99	1.12	1.07	1.10	0.96
1500	1.10	-	1.21	1.05	1.25	1.15	1.23	1.07
2500 ≈ c*	1.14	-	1.27	1.14	1.32	1.30	1.29	1.23

[a]Measurements were carried out at 25 ºC and results are reported as normalized hydrodynamic radii relative to the unfunctionalized chains (for which at 500 ppm R_h = 25.2 nm in Jet-A and 47.9 nm in CDD). The standard deviation of measurements was < 2% of the measured value in all cases. [b]The degree of functionalization with 3-mercaptopropionic acid, as indicated in Table 2.1.

2.7 References and Notes

1. Knight, J. *Antimisting additives for aviation fuels*. United States patent 4,396,398, 1983.

2. Peng, S. T. J.; Landel, R. F., Rheological behavior of progressively shear-thickening solutions. *Journal of Applied Physics* **1981,** 52, (10), 5988–5993.

3. Peng, S. T. J.; Landel, R. F., Rheological behavior of FM-9 solutions and correlation with flammability test results and interpretations. *Journal of Non-Newtonian Fluid Mechanics* **1983,** 12, (1), 95–111.

4. Rodd, L. E.; Scott, T. P.; Cooper-White, J. J.; McKinley, G. H., Capillary break-up rheometry of low-viscosity elastic fluids. *Applied Rheology* **2005,** 15, (1), 12–27.

5. Anna, S. L.; McKinley, G. H., Elasto-capillary thinning and breakup of model elastic liquids. *Journal of Rheology* **2001,** 45, (1), 115–138.

6. Bathel, B. F.; Stephen, N.; Johnson, L.; Ratner, A.; Huisenga, M., Prediction of postcontact parameters of fluid droplet impact on a smooth surface. *AIAA Journal* **2007,** 45, (7), 1725–1733.

7. The extent of MPA incorporation was determined upon analysis of ^{1}H NMR spectra by integration of backbone and side-group peaks, with the following complication. For PB functionalization with MPA, we expect two peaks between 2.85 and 2.55 ppm corresponding to $HO_2CC\mathbf{H_2}CH_2S$- protons and $HO_2CCH_2C\mathbf{H_2}S$-, with one or more additional peaks (depending on whether cyclic structures are formed or not) around 2.55 ppm, corresponding to $HO_2CCH_2CH_2SC\mathbf{H_2}$- protons. Experimental results consistently showed two large, partially overlapping peaks between 2.825 and 2.575 ppm, and a much smaller, broad overlapping shoulder below 2.575 ppm, extending in some cases down to 2.4 ppm (for instance, for 510kPB4.7A polymer that shoulder peak was about 1/3 of the size of the first two). These observations indicate that the signal for $HO_2CCH_2CH_2SC\mathbf{H_2}$- is broad, with significant overlap with the middle peak, and that for simplicity the 2.85-2.4 ppm range should be integrated as a whole, accounting for 6 protons for each functionalized monomer. The complication is that the integration of the small shoulder region between 2.55 and 2.4 ppm was found to be completely unreliable (due both to its small size at the very low extents of functionalization investigated, and apparently to the presence of the very large neighboring PB backbone peak): in many cases, the software-computed integral was a physically nonsensical negative number. As a result, extents of MPA functionalization were calculated instead in all cases by integrating between 2.825 and 2.575 ppm and estimating that that integral accounted for 5 protons for each functionalized monomer.

8. Davis, M. M., In *Acid-Base Behavior in Aprotic Organic Solvents*, 1968; pp. 31–37.

9. Alessi, P.; Cortesi, A.; Sacomani, P.; Valles, E., Solvent Polymer Interactions in Polybutadienes. *Macromolecules* **1993,** 26, (23), 6175–6179.

10. $\eta_{sp} = 2.5\phi$ for non-interacting, rigid, spherical particles dispersed in a liquid medium, meaning that the particles' contribution to solution viscosity depends only their total volume fraction in solution ϕ, and is independent of their size.

11. Rubinstein, M.; Semenov, A. N., Thermoreversible gelation in solutions of associating polymers. 2. Linear dynamics. *Macromolecules* **1998,** 31, (4), 1386–1397.

12. Rubinstein, M.; Semenov, A. N., Dynamics of entangled solutions of associating polymers. *Macromolecules* **2001,** 34, (4), 1058–1068.

13. Semenov, A. N.; Rubinstein, M., Thermoreversible gelation in solutions of associative polymers. 1. Statics. *Macromolecules* **1998,** 31, (4), 1373–1385.

14. Schulz, D. N.; Bock, J., Synthesis and fluid properties of associating polymer systems. *Journal of Macromolecular Science—Chemistry* **1991,** A28, 1235–1243.

15. Schulz, D. N.; Kitano, K.; Duvdevani, I.; Kowalik, R. M.; Eckert, J. A., Hydrocarbon-soluble associating polymers as antimisting and drag-reducing agents. *ACS Symposium Series* **1991,** 462, 176–189.

16. A semi-Markov chain is a stochastic process that takes on a finite number of states, that moves from one state to the next according to transition probabilities P_{ij} (P_{ij} is the probability to transition from state i into state j), and such that the amount of time it spends in any state i, before proceeding to the next state, is a random variable with distribution T_i. When the time spent in every state is always 1, the semi-Markov process is just a Markov chain.

17. Kowalik, R. M.; Duvdevani, I.; Peiffer, D. G.; Lundberg, R. D.; Kitano, K.; Schulz, D. N., Enhanced drag reduction via interpolymer associations. *Journal of Non-Newtonian Fluid Mechanics* **1987,** 24, (1), 1–10.

18. The Zeigler-Natta method of polymerization used in the preparation of the materials characteristically results in very high product polydispersity.

19. Stadler, R.; Freitas, L. D., Complex-formation and dynamics in polymer melts. *Makromolekulare Chemie—Macromolecular Symposia* **1989,** 26, 451–457.

20. Rubinstein and Semenov's model describes the static and dynamic properties of solutions of linear chains randomly functionalized with pairwise, self-associating groups. They assumed monodisperse chains of N Kuhn monomers, containing f stickers capable of forming pairwise associations of energy εkT, located at constant intervals (i.e., separated by $l = N/f$ monomers) along the entire chains. For entangled polymer chains with strongly associating stickers, above the gel point and in good solvent, the model predicts a rich cascade of scaling regimes in the concentration dependence of viscosity shown in Figure 2.17 (Rubinstein, M.; Semenov, A. N. *Macromolecules* **2001,** 34, (4), 1058-1068). Transitions from one regime to another are predicted to occur at the entanglement concentration ϕ_e, the overlap concentration of the strands between stickers ϕ_s, the entanglement concentration of the strands between stickers ϕ_{le}, and a crossover concentration ϕ_r above which the lifetime of bonds must be renormalized to account for reassociation of the same pair of separated stickers due to a shortage of free partners. Below ϕ_s, any sticker's closest partners in space are its neighbors on the same chain, so interactions are mostly intramolecular. The steep increase in viscosity with concentration between ϕ_e and ϕ_s corresponds to a transition from predominantly intramolecular to predominantly intermolecular pairing. For comparison, the concentration dependence of viscosity for linear, non-associating chains is $\eta \sim \phi^{1.3}$ below ϕ_e and $\eta \sim \phi^{3.9}$ above ϕ_e according to de Gennes' reptation model. We note that the $\eta \sim \phi^{5.3}$ relationship which we observed above ϕ_e for unmodified PB is consistent with the well-known observation that the simple reptation model underestimates the value of the exponent for real chains (Rubinstein, M.; Colby, R. H., In *Polymer Physics*, Oxford: 2003; p 374).

21. Obtained using published equilibrium constants of associations (Davis, M. M., In *Acid-Base Behavior in Aprotic Organic Solvents*, 1968; pp 31–37) as explained in Section 4.5.6.

22. Obtained for 510kPB chains in CDD by rearrangement of the scaling relation $\phi^* \approx (b^3/v)^{6\nu-3} N^{1-3\nu}$ (Rubinstein, M.; Colby, R. H., In *Polymer Physics*, Oxford: 2003; Equation 5.19, p 176), using swelling exponent $\nu \approx 0.588$ and overlap concentration $\phi^* \cong 0.003$. In the above equation, v is the excluded volume parameter and b is the Kuhn monomer length. The number of Kuhn monomers N was estimated for chains of $M_w \sim 510$ kg/mol assuming Kuhn monomers of molecular weight ~ 100 g/mol.

23. The overlap concentration of a segment of size N monomers scales with $N^{1-3\nu}$, where the fractal exponent is $\nu \approx 0.588$ in good solvent.

24. Peng, S. T. J.; Landel, R. F., Preliminary Investigation of Elongational Flow of Dilute Polymer-Solutions. *Journal of Applied Physics* **1976,** 47, (10), 4255–4260.